Journal of Experimental Botany, Vol. 69, No. 3 pp. 525–535, 2018
doi:10.1093/jxb/erx405 Advance Access publication 23 December 2017
This paper is available online free of all access charges (see http://jxb.oxfordjournals.org/open_access.html for further details)

RESEARCH PAPER

Novel computed tomography-based tools reliably quantify plant reproductive investment

Y. M. Staedler[1,†,*], T. Kreisberger[1,†], S. Manafzadeh[1,†], M. Chartier[1,†], S. Handschuh[2], S. Pamperl[1], S. Sontag[1], O. Paun[3] and J. Schönenberger[1]

[1] Department of Botany and Biodiversity Research, Division of Structural and Functional Botany, University of Vienna, Austria
[2] VetCORE – Facility for Research, University of Veterinary Medicine Vienna, Veterinärplatz 1, 1210 Vienna, Austria
[3] Department of Botany and Biodiversity Research, Division of Systematic and Evolutionary Botany, University of Vienna, Austria

[†] These authors contributed equally to this work.
[*] Correspondence: yannick.staedler@univie.ac.at

Received 4 September 2017; Editorial decision 17 October 2017; Accepted 19 October 2017

Editor: Daphne Goring, University of Toronto, Canada

Abstract

The flower is a bisexual reproductive unit where both genders compete for resources. Counting pollen and ovules in flowers is essential to understand how much is invested in each gender. Classical methods to count very numerous pollen grains and ovules are inefficient when pollen grains are tightly aggregated, and when fertilization rates of ovules are unknown. In this study we have therefore developed novel counting techniques based on computed tomography. In order to demonstrate the potential of our methods in very difficult cases, we counted pollen and ovules across inflorescences of deceptive and rewarding species of European orchids, which possess both very large numbers of pollen grains (tightly aggregated) and ovules. Pollen counts did not significantly vary across inflorescences and pollination strategies, whereas deceptive flowers had significantly more ovules than rewarding flowers. The within-inflorescence variance of pollen-to-ovule ratios in rewarding flowers was four times higher than in deceptive flowers, possibly demonstrating differences in the constraints acting on both pollination strategies. We demonstrate the inaccuracies and limitations of previously established methods, and the broad applicability of our new techniques: they allow measurement of reproductive investment without restriction on object number or aggregation, and without specimen destruction.

Keywords: Deceptive orchids, machine counting, micro computed tomography, ovule count, pollen count, pollination.

Introduction

It should be evident to most human beings that the mere existence of genders is a harbinger of conflicts for resources. Gender conflicts are nowhere more acute than in hermaphroditic organisms where both genders have to draw from the resource pool of the same organism to maximize fitness (Charnov, 1979; Lloyd, 1979). In the overwhelmingly hermaphroditic flowering plants, counting the pollen grains and ovules of flowers allows us to understand how much a plant invests in the male versus female part of its fitness.

Pollen counting methods fall into three groups (Costa and Yang, 2009): counting with the naked eye, particle counters, and image-processing algorithms. Counting visually usually involves spreading samples on specialized slides with a grid and counting a sub-sample (e.g. Jorgensen, 1967; Kearns and Inouye, 1993), which is then extrapolated (Kannely,

© The Author(s) 2017. Published by Oxford University Press on behalf of the Society for Experimental Biology.
This is an Open Access article distributed under the terms of the Creative Commons Attribution License (http://creativecommons.org/licenses/by/4.0/), which permits unrestricted reuse, distribution, and reproduction in any medium, provided the original work is properly cited.

2005). Pollen grains tend to settle disproportionately on grids, especially if the grains are large or still aggregated, which may then produce incorrect estimates (Kannely, 2005). Electronic or laser-based counters physically detect pollen grains in order to count them. A particle counter counts every particle; unfortunately, this may include debris and aggregated pollen (Kearns and Inouye, 1993). Image processing automates pollen counting from pollen grain images. This requires software to scan the images for objects and then count each object as a unit (e.g. Bechar *et al.*, 1997; Aronne *et al.*, 2001). All three approaches require sample destruction, including proper de-aggregation of the grains, which can be hard to achieve.

Ovules are counted either before fertilization (as ovules) or after fertilization and maturation (as seeds). At the ovule stage, counting is manual after dissection, either directly or on photographs (Nazarov, 1989), either on the whole ovary or on a selected stretch (ovules per mm are then extrapolated to the length of the whole gynoecium). At the seed stage, methods fall into two groups, as follows. (1) Extrapolations based on counting a sub-sample of known weight (Salisbury, 1942), or on a portion of a line of dry seeds (Darwin, 1862), or on the surface of a liquid (Burgeff, 1936), or within a suspension of seeds (Proctor and Harder, 1994; Sonkoly *et al.*, 2016). (2) Use of particle-counting devices (DuBois, 2000). All these approaches require sample destruction and rely on the assumption that all ovules have been fertilized, which is hard to test.

In summary, these traditional methods for counting pollen and ovules show limitations with very large numbers of pollen grains (that are tightly aggregated) and ovules (especially when fertilization rates are unknown). Given these limitations, novel and more reliable methods to count pollen and ovules are needed. Contrast agents used in X-Ray computed tomography (CT), especially phosphotungstic acid, semi-selectively accumulate in both pollen and ovules, possibly due to the higher protein content of their cells/tissues relative to their surroundings (Hayat, 2000; Staedler *et al.*, 2013; Bellaire *et al.*, 2014). By selecting only the brightest voxels (3D pixels) of the 3D model, i.e. the areas that absorb the most X-Rays (X-Ray data are traditionally displayed in negative), it is possible to segregate pollen and ovules from their surroundings tissues. This process is called greyscale thresholding. Obtaining the volume of such a selection by counting voxels is straightforward. Provided that the average volume of a grain or ovule is available, CT can thus be used to count ovules and pollen in cases where classical methods are at their limits.

These limits are nowhere more evident than in the study of orchids, which both possess enormous numbers of ovules and (tightly aggregated) pollen grains (Darwin, 1862). Orchids are remarkable plants in many ways: not only are they the largest family of flowering plants (with up to 30 000 species), but also almost a third of them offer no reward to their pollinators (Porsch, 1909; Van der Pijl and Dodson, 1966; Ackerman, 1986). The presence of a reward, or lack thereof, dramatically influences pollinator behaviour: in rewarding taxa, the pollinators tend to visit several or all open flowers of an inflorescence during a visit, and visit the same inflorescence repeatedly in order to harvest its rewards (Van der Cingel, 1995; Fig. 1A, B). In taxa with deceptive flowers, however, pollinators tend to learn to avoid deception and to visit only the first open flowers they encounter while they are still naive (Jersáková and Kindlmann, 1998; Van der Cingel, 1995; Fig. 1D). Consequently, in rewarding plants the fruit set is usually higher and the fruits are spread across the inflorescence (Neiland and Wilcock, 1995; Fig. 1C), whereas in deceptive plants only the first flowers to open tend to bear fruit (Nilsson, 1980; Vogel, 1993; Jersáková and Kindlmann, 1998; Fig. 1E). In orchids in general, the ratio of pollen to ovules (P:O) increases from the bottom to the top of inflorescences (Salisbury, 1942; Nazarov and Gerlach, 1997; Kopylov-Gus'kov Yu *et al.*, 2006). Due to decreased pollinator visits to the top flowers, we hypothesise that the decrease in ovule number (increase in P:O) should be stronger across inflorescences of deceptive flowers than across inflorescences of rewarding flowers (Fig. 1F–I). The Orchidinae, to which most European orchids belong, are a good system to test this hypothesis because their pollination biology and phylogenetic relationships are very well understood (Van der Cingel, 1995; Claessens and Kleynen, 2011; Inda *et al.*, 2012). The phylogenetic relationship between the species studied needs to be known in order to control for potential phylogenetic constraints.

This study was aimed at: (1) establishing new methods for pollen and ovule counting that can be used even for flowers with many, densely aggregated pollen grains and ovules; and (2) demonstrating the potential of these methods by focussing on species of European orchids to determine whether the differences of pollinator behaviour in rewarding versus deceptive plants lead to different patterns of reproductive investment at the level of the inflorescence.

Materials and methods

Plant material

We sampled three rewarding and five deceptive species of the subtribe Orchidinae (Inda *et al.*, 2012; see Supplementary Table S1 at *JXB* online). We collected three flowers for 2–4 inflorescences per species, for a total of 76 flowers (see Supplementary Table S2).

Collection method

Open flowers (including pollinia, i.e. the pollen aggregates of orchids) or buds close to anthesis were collected from the bottom, middle, and top sections of inflorescences and were immediately fixed in 1% phosphotungstic acid (the contrast agent) in formalin–acetic acid–alcohol (1% PTA / FAA; Fig. 2A). The flowers were removed from the plants using razor blades and tweezers.

Sample preparation

The sampled flowers and buds were de-aerated for 20–30 min using a water-jet vacuum pump. Total infiltration time in 1% PTA / FAA was 4–6 weeks during which the solution was changed twice. The long infiltration time allowed saturation of the sample with the contrast agent. In order to further optimize for space constraints during mounting for CT-scanning and to prevent the formation of

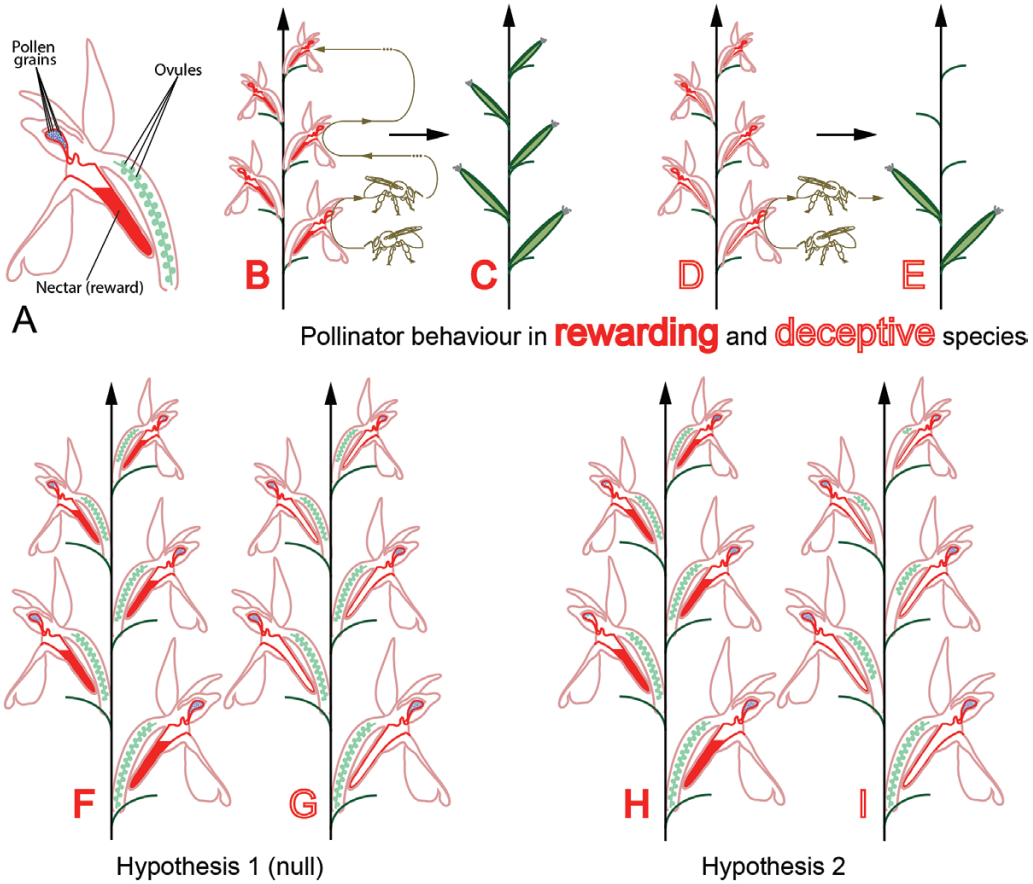

Fig. 1. Pollinator reward or deception lead to different fruit set: hypotheses on reproductive investment. (A) Diagram of orchid flower. (B) Schematic behaviour of a pollinator on a rewarding inflorescence: the pollinator learns to associate the flowers with reward and visits the inflorescence repeatedly. (C) Fruit set in rewarding inflorescences is equally distributed on the inflorescence. (D) Schematic behaviour of a pollinator on a deceptive inflorescence: a naive pollinator soon learns to avoid such inflorescences. (E) Fruit set on a deceptive inflorescence is concentrated on the first flowers to open, at the bottom of the inflorescence. (F, G) Hypothesis 1: there is no difference between gender allocation strategy in deceptive and rewarding inflorescences. (H, I) Hypothesis 2: there is a difference between gender allocation strategies of deceptive and rewarding inflorescences. The difference in reproductive investment between lower and higher flowers is stronger in deceptive inflorescences than in rewarding inflorescences.

air bubbles, the petals and sepals were removed with tweezers and dissecting scissors (Fig. 2B). The mounting was then performed in a 200-µl pipette tip (Standard UNIVERSAL, Art. No.: B002.1, Carl Roth GmbH+Co KG) as described in Staedler *et al.* (2013) with the following differences. (1) Before mounting, the bottom end of the pipette tip was cut off. This allowed us to enter the tip with a preparation needle and to drag down the samples to optimize the space used without displacing or breaking pollinia. (2) The samples were not washed with 70% ethanol before scanning, but immediately mounted in PTA / FAA (Fig. 2C). The singly-mounted flowers were then batched in longitudinally slit tubes of kapton (an X-Ray lucent material; see Fig. 2D; diameter ~3 mm, American Durafilm Co., Inc.). Although the tension produced by the shape of the tubes stabilized the samples, they were additionally stabilized by gluing them to the slit tubes with epoxy glue (UHU Plus, UHU GmbH & Co. KG). The batch was then placed in an in-house batch holder and fixed with epoxy glue, itself fixed to the sample table (see Fig. 2E). Epoxy glue was then added between all the above-mentioned parts to stabilize them. In this way, we were able to programme and scan batches of up to five flowers sequentially.

Scanning

Scanning was performed with a MicroXCT-200 system (Zeiss Microscopy). Scanning conditions are summarized in Supplementary Table S2. 3D reconstructions were performed via the software XMReconstructor 8.1.6599 (Zeiss Microscopy). In order to have repeatable greyscale values from one scan to another, byte scaling and CT scaling were used. Byte scaling is a procedure in which minimum and maximum greyscale values are set for the whole reconstructed scan volume (Xradia, 2010); this procedure was used for the reconstruction of scans of gynoecia. CT scaling is a procedure by which greyscale values are scaled to the values of two reference materials (Candell, 2009); in our studies, air and a solution of 1% PTA in FAA were used. CT scaling requires scanning of a dummy (or phantom) filled with the reference material and the presence of air on both sides of the sample during the whole scan (Fig. 2F). For this reason, a pipette tip was filled with FAA+PTA, sealed on the bottom end with paraffin wax, shortened at the top, and sealed with parafilm (Fig. 2F). For a single dummy scan to be used on multiple sample scans, the following parameters have to remain constant: number of projection images, voltage, objective type, beam hardening coefficient, and source filter (Candell, 2009; Fig. 2G). In practice, for all the scans in which we used CT scaling, projection images, objective type, beam hardening coefficient, and source filter were constant, whereas only voltage varied (see Supplementary Table S2). We therefore carried out a new dummy scan for each new voltage value.

Calibration was performed as described in the system's manual (Candell, 2009). The density of FAA+PTA was measured seven times by using either a 100-ml measuring cylinder (four measurements) or a 50-ml cylinder (three measurements) and an arithmetic mean of 93.7 g 100 ml^{-1} was determined and used for calibration. Pollinia were reconstructed with CT scaling.

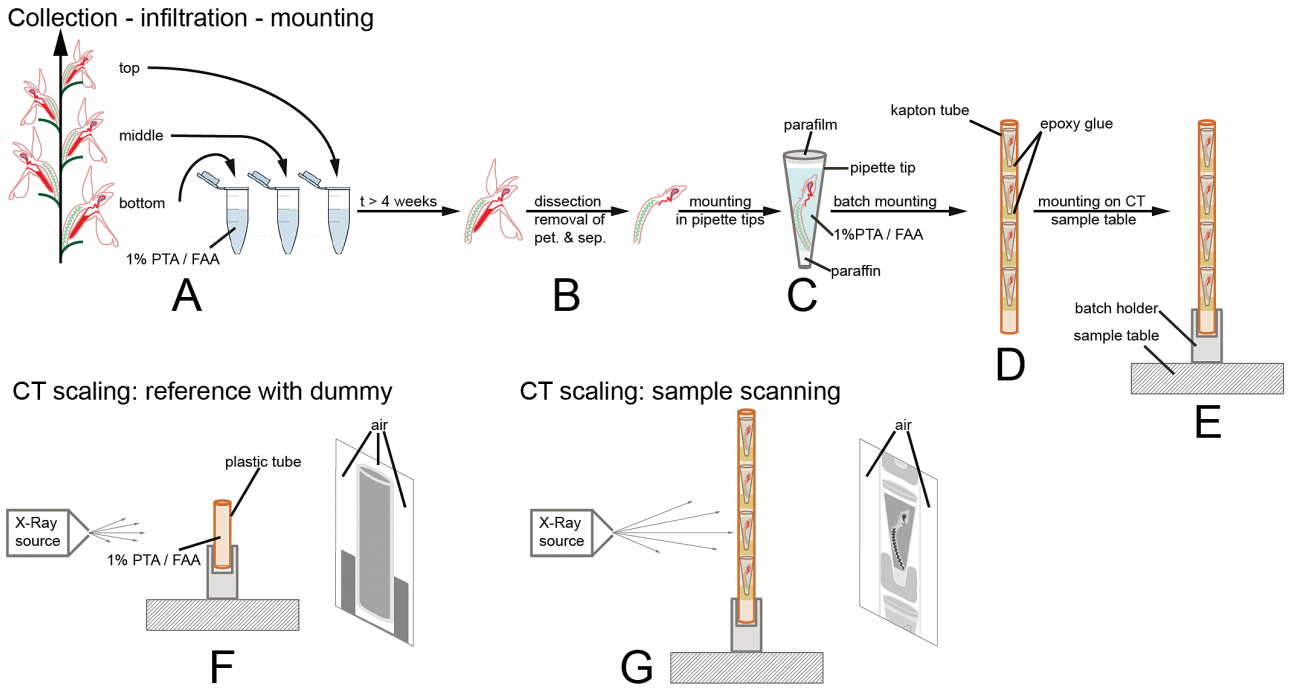

Fig. 2. Sample processing and scanning approach. (A) Collection and fixation of flowers. (B) Removal or perianth organs of flowers. (C) Mounting in pipette tip. (D) Mounting in batches in kapton tubes. (E) Mounting on sample table for scanning. (F) Scanning of dummy for CT scaling, in order to obtain calibrated greyscale values (air has to be in the field of view on both sides and on top of the sample). (G) Sample scanning. Air has to be present on both sides of the sample for CT scaling to work.

Data processing

Two different procedures were developed to count pollen (summarized in Fig. 3A–D) and ovules (summarized in Fig. 3E–I). The pollen count procedure involves a high- and a low-resolution scan. In the low-resolution scan, the whole pollinium is visible so that the whole pollen volume is accessible; however, in this scan individual pollen grains are not resolved due to their strong aggregation. A high-resolution scan (Fig. 3B) is thus used to estimate the number of pollen grains in a domain of the low-resolution scan (Fig. 3C), which is then extrapolated to the whole pollinium (Fig. 3D). The estimation of the pollen grain number in the high-resolution scan is performed via a series of thresholding and image-processing steps followed by automatic object counting (summarized in Fig. 4, and detailed below).

The images of the high-resolution scan were imported into the data analysis software AMIRA 5.4.1 [Build 006-Se11b; Konrad-Zuse Zentrum Berlin (ZIB) and Visage Imaging Inc.]. The raw data (Fig. 4A, B) was first thresholded (Fig. 4C, D), i.e. all data below a threshold value of greyscale were removed from the dataset. The data were then filtered via a 3D median filter (kernel size 3×3×3 voxels; see Fig. 4E, F) and a Gaussian smoothing filter (kernel size 9×9×9 voxels; Fig. 4G, H). The images were then exported as 3D TIFF files to Fiji (Schindelin *et al.*, 2012), a distribution of ImageJ (Schneider *et al.*, 2012; https://imagej.nih.gov/ij/). Single pollen grains were then separated via '3D Iterative Thresholding' (Ollion *et al.*, 2013; Fig. 4I, J), thresholded (Fig. 4K, L), and counted with the '3D Object Counter' (Bolte and Cordelières, 2006). Subsequently, the pollen volume of the subset of the high-resolution scan was measured in the low-resolution scan (via the cropping function; Fig. 3C). Finally, we calculated the number of pollen grains per pollen volume for the low-resolution scan, and extrapolated that value to the whole flower (Fig. 3D) in order to obtain the total pollen grain number.

The ovule count procedure only involved one scan because the ovules can be distinguished on scans of the whole gynoecium. The ovules were segmented away from the rest of the ovary (Fig. 3E–G). A subset was selected (Fig. 3H) and the ovules were counted manually by using the landmark function in AMIRA (Fig. 3I). The average ovule volume was thereby calculated. The total ovule volume was then divided by the average volume of one ovule in order to obtain total ovule number per flower.

Statistical tests

We investigated differences in the number of ovules, the number of pollen grains, and the value of the pollen-to-ovule ratio (P:O) between rewarding and deceptive species, among species, and within inflorescences. We therefore tested the effects of the factors 'interaction' (deceptive and rewarding), 'species', and 'flower position' (bottom, middle, and top) on the number of ovules, on the number of pollen grains, and on the P:O per flower, respectively. Analyses were performed with the R software (R Core Team, 2016). Because our data are non-parametric (see Supplementary Data S1), we used a non-parametric analysis of variance (npANOVA), with the function *adonis* of the vegan package (Oksanen *et al.*, 2013). We first generated a distance matrix with the function *dist* of the stats package using the Euclidean distance index, and then performed the npANOVA using 9999 permutations (Anderson, 2001). *Post hoc* tests were performed with the same function, with a Bonferroni correction for multiple comparisons. Finally, we used the same test to look for an effect of the interaction between the factors 'species' and 'flower position': if the effect is significant, it means that the number of pollen or ovules does not vary in the same direction within the inflorescence for each species. If this effect is not significant, it means that the number of ovules or pollen grains varies in the same direction within the inflorescences for all species. The variance of the P:O per species was compared between rewarding and deceptive species with a non-parametric Mann–Whitney–Wilcoxon (MWW) test using the function *wilcox.test* of the stats package.

Phylogenetic analyses

We used a pruned version of the time-calibrated phylogeny of Inda *et al.* (2012) for phylogenetic comparative analyses (Fig. 5E). We did not include *Dactylorhiza majalis* in our phylogeny, because of

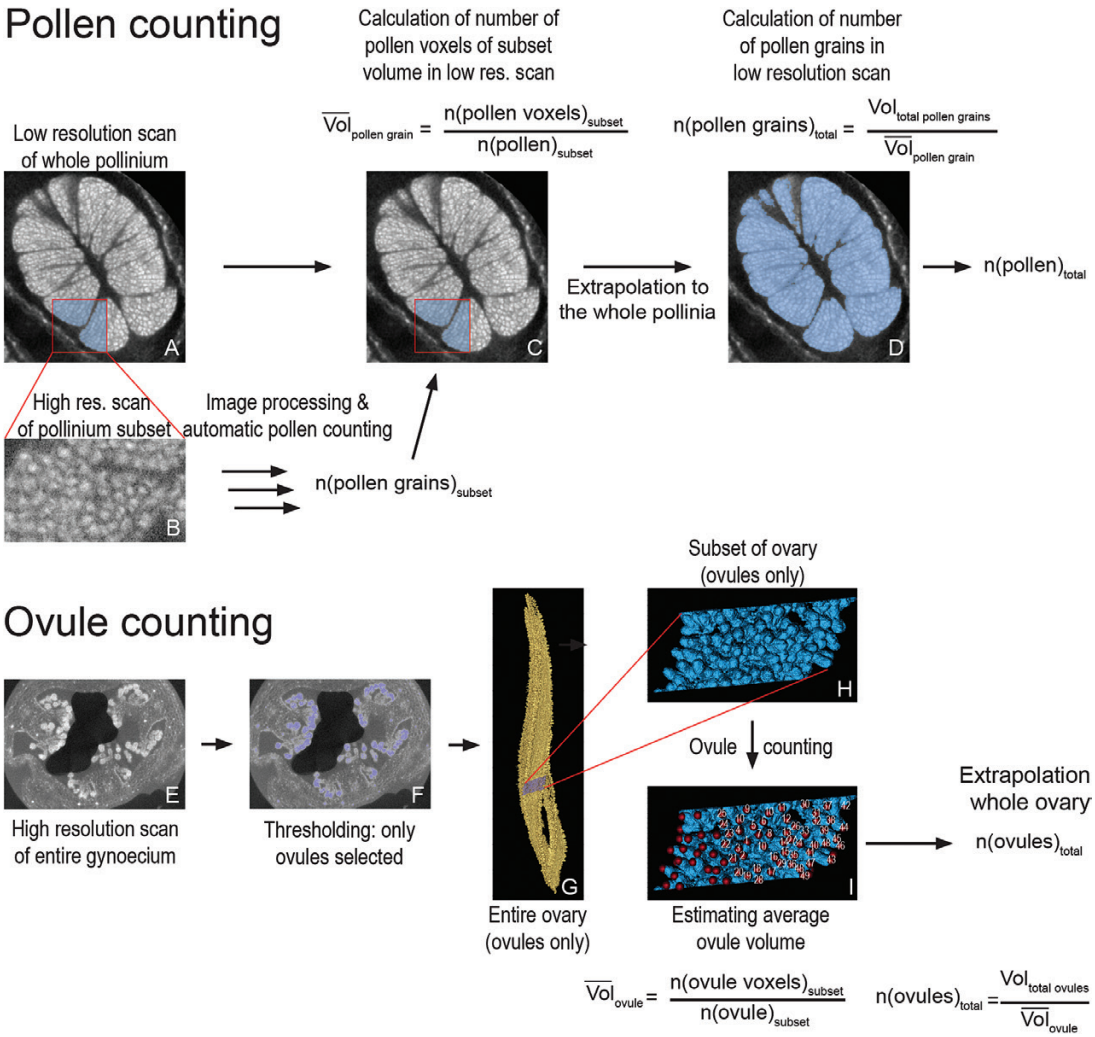

Fig. 3. Workflows for object counting. (A–D) Workflow for counting when individual objects cannot be resolved on a scan of the whole tissue, e.g. pollen in orchid pollinium. (A) Reconstructed section through a pollinium with the subset area highlighted in blue. (B) Reconstructed section of a high-resolution scan of the subset area (raw data). After image processing and automated object counting, the number of grains in the subset is calculated. (C) The number of pollen grains in the subset is used to calculate the average volume of a pollen grain in the overview scan. (D) The average volume of a pollen grain in the overview scan is used to calculate total pollen grain number. (E–I) Workflow for counting when individual objects can be resolved on a scan of the whole tissue, e.g. ovules in orchid ovary. (E) Reconstructed section through ovary. (F) Thresholding of ovules in ovary (section). (G) Thresholding of ovules in ovary (3D model), with the subset highlighted in blue. (H) 3D model of the subset. (I) Counting of ovules in the subset (using the landmark function in AMIRA, which registers how many points have been set). This count allows the estimation of the average volume of a single ovule. This value is then used to obtain the total ovule number.

its allotetraploid origin (Hedrén *et al.*, 2001). First, we calculated the amount of phylogenetic signal in individual traits using the maximum-likelihood value of Pagel's λ (Pagel, 1999). We estimated Pagel's λ using the function *fitContinuous* based on likelihood optimisation (ML) for four continuous traits and *fitDiscrete* based on the symmetric model (SYM) for one discrete trait, in the geiger package (Harmon *et al.*, 2008). λ=0 indicates that there is no phylogenetic signal for the trait, which means that the trait has evolved independently of phylogeny, i.e. close taxa are not more similar on average than distant taxa. λ=1 indicates that there is a strong phylogenetic signal, which means that the trait has evolved according to the Brownian motion model of evolution (Pagel, 1999).

We also applied phylogenetic generalized least-squares (PGLS; Martins and Hansen, 1997) to understand the nature of the evolutionary association between biological traits, as implemented in the caper package (Orme, 2013). We identified one predictor variable (presence/absence of floral reward) that could affect the response variables (pollen grain number, ovule number, P:O, and variance thereof) and ran a PGLS including all the variables. First, a variance–covariance matrix was calculated based on the phylogenetic relationships of the species. In the PGLS, λ applies to the residual errors from the regression model, not to the strength of the signal in the response variable, nor to that of the predictor variables. λ=0 indicates a non-phylogenetic covariance matrix, whereas λ=1 refers to the expected phylogenetic covariance matrix under a Brownian motion model of evolution (Garamszegi, 2014).

Results

Development of a new method

We present a set of two approaches to count numerous high-contrast objects in plant tissues via X-Ray CT. One method is presented for cases where it is possible to resolve all the objects to be

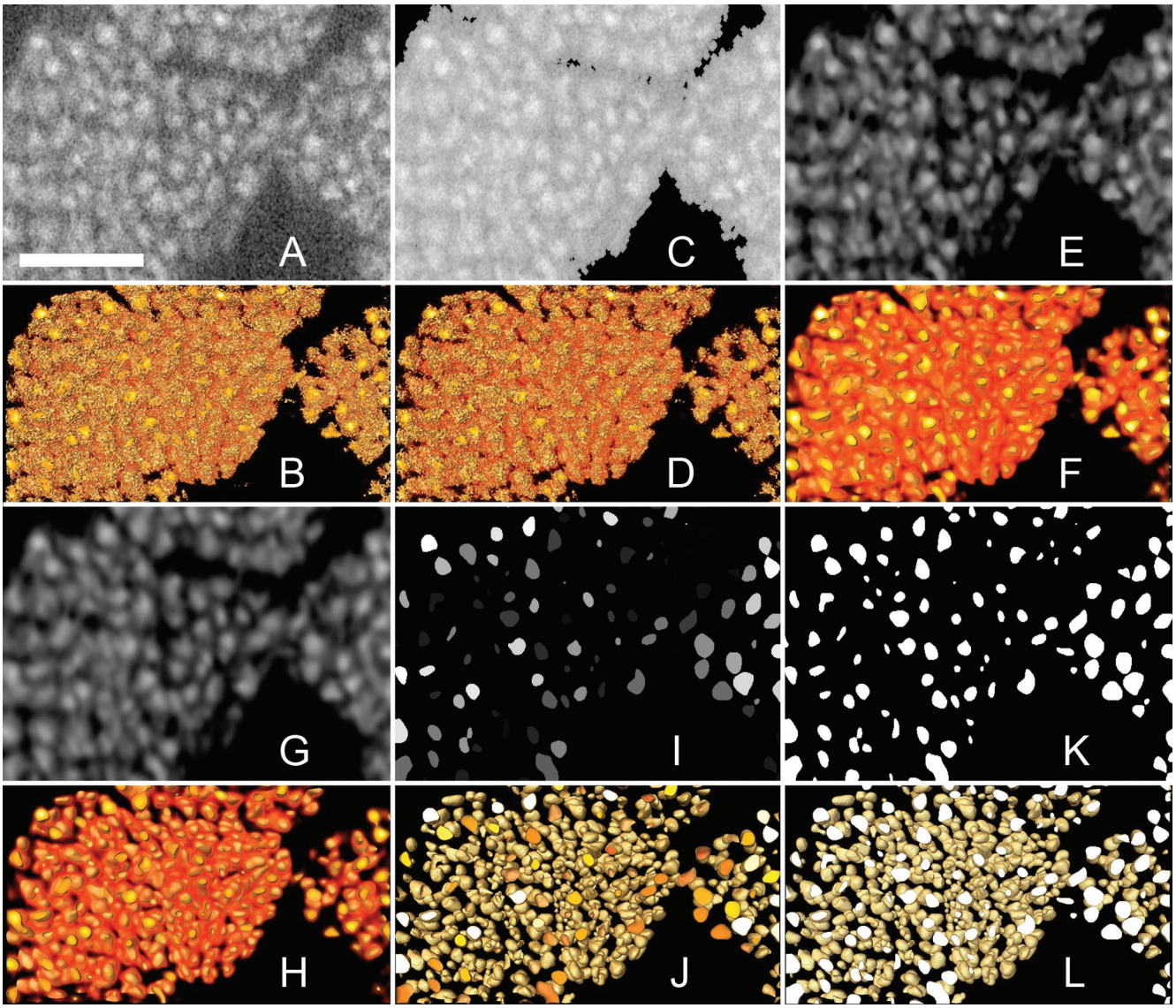

Fig. 4. Image processing pipeline. Sections through the high-resolution scan dataset of the pollinium subset and associated 3D models illustrating the sequence of steps during image processing. (A) Reconstructed section of raw data. (B) 3D model of the raw data. (C) Data after greyscale thresholding (removal of voxels darker than a specific value). (D) 3D model of the data after greyscale thresholding. (E) Data after the 3D median noise reduction filter. (F) 3D model of data after the 3D median noise filter. (G) Data after the 3D Gaussian smoothing filter. (H) 3D model of data after the 3D Gaussian smoothing filter. (I) Data after iterative thresholding. (J) 3D model of data after iterative thresholding. (K) Data after greyscale thresholding. (L) 3D model of the data after greyscale thresholding. The number of objects in the scan data can now be automatically counted with the 3D Object Counter function of Fiji. Scale bar = 50 µm. An animation of the process is provided in Supplementary Movie S1.

counted on a scan of the whole tissue. The other method is applicable when this is not the case. Ovules can be resolved on scans of the whole ovary, and therefore an estimation of the average volume of an ovule and an ovule count can be carried out on the same data (Fig. 3E–I). At least in the special of case of Orchidaceae, where pollen grains are relatively small and aggregated in compact pollinia, individual pollen grains cannot be resolved on the same scan data as overview scans of the entire pollinium. Two scans are therefore necessary (see Fig. 3A–D). A high-resolution scan of a subset of the tissue has to be performed in order to estimate the number of pollen grains inside this subset (Fig. 3B, C); this number will then be used to estimate the total object number in the overview scan (Fig. 3D). On the high-resolution scan, image processing and automatic counting methods are presented that allow the straightforward processing of scan data (Fig. 4).

Variation of number of pollen grains and massulae per flower

Pollen grain number per flower significantly differed among species (npANOVA: F=34.32, R^2=0.81, P=0.001; Table 1) and ranged from 35 588 ± 2 823 in *Dactylorhiza viridis* to 215 978 ± 25 687 in *Platanthera bifolia*. There was no significant difference in pollen grain number per flower between rewarding and deceptive species (npANOVA: F=0.02, R^2=0.00, P=0.918), and the number of pollen grains per flower did not significantly differ within inflorescences (npANOVA: F=0.7, R^2=0.01, P=0.520). This lack of significance is probably due to our small sample size. In fact, when looking at the data, pollen grain number tended to increase from bottom to top in *Orchis militaris* and *D. fuchsii*, and to decrease from bottom to top in *P. bifolia*,

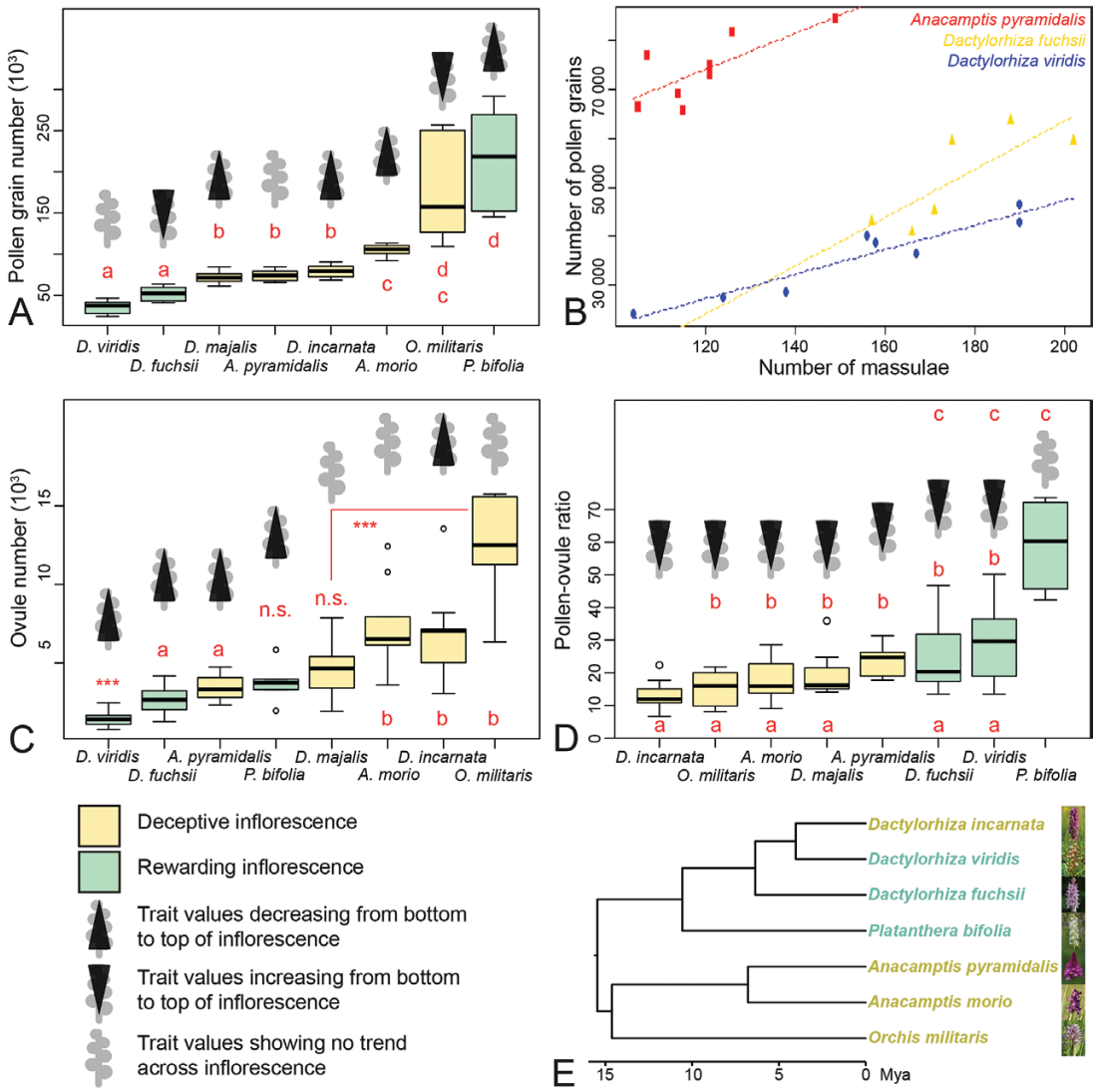

Fig. 5. Pollen, massulae, ovules, pollen:ovule ratio, and phylogeny. (A) Pollen grain number per flower for the eight orchid species studied. (B) Massulae number per flower and corresponding pollen grain numbers for a subset of three species. (C) Ovule number per flower for the eight orchid species studied. (D) P:O per flower for the eight orchid species studied. (E) Time-calibrated phylogeny of the eight orchid species studied (modified from data in Inda *et al.*, 2012). (A, C, –D) Data displayed in boxplot format. Letters indicate species that group together accordin g to the npANOVA *post hoc* tests. ***, Group that differs from all the others, or significant differences between two groups; n.s., group that differs from none of the others.

D. majalis, *D. incarnata*, and *Anacamptis morio*. There was no trend of variation in *D. viridis* and *A. pyramidalis* (Fig. 5A).

The number of massulae (sub-aggregates within the pollinium) per flower was determined for *A. pyramidalis*, *D. fuchsii*, and *D. viridis* (see Supplementary Table S3). The number of massulae per flower ranged between 105–149 in *A. pyramidalis*, between 157–202 in *D. fuchsii*, and between 104–190 in *D. viridis*. A positive correlation between number of massulae per flower and the total number of pollen grains was apparent (Fig. 5B). In two species this correlation was significant: in *A. pyramidalis* ($F_{1,6}$=7.77, P=0.03168, R^2=0.4916) and in *D. viridis* ($F_{1,6}$=56.57, P=0.000286, R^2=0.8881), whereas in *D. fuchsii* only a trend could be detected ($F_{1,4}$=6.942, P=0.0579, R^2=0.543).

Variation of ovule number per flower

Ovule number per flower significantly differed among species (npANOVA: F=29.3, R^2=0.45, P=0.001; Fig.5C) and ranged between 1413 ± 134 in *D. viridis* to 12 616 ± 1296 in *O. militaris* (Table 1). Deceptive species produced on average significantly more ovules per flower (6408 ± 521) than rewarding species (2342 ± 248; npANOVA: F=112.5, R^2=0.29, P=0.001). Finally, ovule number per flower tended to decrease from bottom to top of the inflorescences for all species (npANOVA: 'flower position', F=19.5, R^2=0.10, P=0.001; effect of the interaction 'species' × 'flower position', F=1.3, R^2=0.04, P=0.256). This trend was not clear for *A. morio*, *D. majalis*, and *O. militaris* (Fig. 5C).

Pollen/ovule ratio

The P:O per flower significantly differed among species (npANOVA: F=16.28, R^2=0.36, P=0.001; Fig. 5D) and ranged from 13.06 ± 1.70 in *D. incarnata* to 59.08 ± 5.41 in *P. bifolia* (Table 1). The P:O in rewarding species (36.91 ± 4.27) was twice as high as in deceptive species (17.95 ± 1.08; npANOVA: F=112.5, R^2=0.29, P=0.001), and on average more than four times more variable (MWW-test: n_1=3, n_2=5,

W=0, P=0.035; Table 1). Finally, the P:O tended to increase from bottom to top of the inflorescences for all species (npANOVA: 'flower position', F=17.80, R^2=0.12, P=0.001; effect of the interaction 'species' × 'flower position', F=0.91, R^2=0.05, P=0.545). This trend was not clear for *P. bifolia* (Fig. 5D).

Phylogenetic analyses

Individually, the traits used in the analyses exhibited a value of Pagel's λ that was nearly always zero, indicating no phylogenetic signal, except for the 'mean pollen number' (λ=1; see Supplementary Table S4). In contrast to the phylogenetic signal estimates for the individual variables, the estimated maximum likelihood values of λ for two of the regression models ['mean ovule number' ~ 'pollination strategy' (deceptive or rewarding) and 'P:O variance' ~ 'pollination strategy'] were zero, indicating no phylogenetic signal in the residual errors of the models, and hence results that are equivalent to conventional ordinary least-squares analyses. However, two other regression models ('mean pollen grain number' ~ 'pollination strategy' and 'P:O' ~ 'pollination strategy') were under a Brownian motion model of evolution with an estimated maximum likelihood value of λ=1. The 'pollination strategy' was only strongly associated with the 'P:O variance' (see Supplementary Table S5).

Discussion

Development of a new method

Traditionally, pollen and ovule counts have relied on destructive sampling and sub-sampling. For example, pollen counts in orchids have relied on counts of single massulae (sub-aggregates within the pollinium), which are then extrapolated to the whole pollinia (Nazarov and Gerlach, 1997). This method is flawed for two reasons, as follows.

(1) Within a pollinium, massulae have widely different numbers of pollen grains; often there are a few large massulae and many smaller ones. These differences in size have been shown to be stronger in deceptive orchids than in rewarding ones (Nazarov and Gerlach, 1997). This unequal distribution is probably the reason why our counts of pollen grains in the rewarding *P. bifolia*, which has many massulae of similar size, is close to the pollen counts published by Nazarov and Gerlach (1997), whereas in the deceptive *D. incarnata*, the pollinia of which are composed of massulae of widely different sizes, our values are very different from Nazarov and Gerlach (1997). Nazarov and Gerlach (1997) also possibly over-estimated the numbers of pollen grains in *D. incarnata* because, by mostly counting the grains in the few, large massulae, they probably over-estimated the contribution of the many small massulae.

(2) Extrapolating values from massulae assumes that, within the same species, massulae numbers and pollen grain numbers are always tightly correlated, which our data show not to be correct (see Fig. 5B). Counting methods relying on the whole volume of pollen are therefore more precise than methods relying on counts of massulae. Our methods also do not require de-aggregation of the pollen grains. Pollen aggregation has evolved at least 39 times in angiosperms, including in some of their most species-rich lineages (e.g. the legumes and the orchids), probably because it promotes male fitness in response to infrequent pollinator visits (Harder and Johnson, 2008). The counting method we present allows the requirement of de-aggregation of the pollen grains to be bypassed, and can provide accurate counts for any type of pollen.

For the species we studied, the seed counts from the literature were mostly obtained from flowers that were naturally pollinated (see Table 1 and citations therein). We therefore assume that, in species with deceptive flowers, only 10% of all fruit came from flowers from the top third of the inflorescence. In species with rewarding flowers, we assume that the seeds were counted from all portions of the inflorescences equally. With these assumptions, our counts were on average 4.5% higher than the values from the literature (see Table 1 and citations therein), although the variation was very large and this makes comparisons difficult. Our higher counts were probably due to our method of counting all ovules, not only those that were fertilized. We could not test for the latter due to the specificities of orchid seed development, and the specifics of the contrast agent used in this study (see Appendix S1). In the gynoecia of flowers at the top of inflorescences, extensive gaps in the ovule distribution were often noticed (see Supplementary Fig. S1A–E). These gaps could affect the chemotactic signalling from the ovules to guide pollen tubes (Okuda *et al.*, 2009; Takeuchi and Higashiyama, 2016), which could lead to some ovules not being fertilized, even if the pollen loads would be sufficient to do so.

And finally, unlike all the previously existing methods that require the destruction of the sample, our processing methods allow the measurement of both pollen and ovule numbers from the same flower with minimal destruction (perianth removal). The column and ovary are left intact after counting, and could be used for other analyses: e.g. shape analysis, histology, etc. The methods we present are flexible and could be used to count any high-contrast objects inside plant tissues, such as crystals (druses or raphides) or stone cells (sclereids).

Reproductive investment and presence/absence of floral reward

There was no significant difference in pollen grain number per flower between rewarding and deceptive species, probably because two rewarding species, *D. viridis* and *D. fuchsii*, produced significantly less pollen than all the other species, whereas the third rewarding species, *P. bifolia*, was one of the species producing the most pollen grains per flower (Fig. 5A). There were also no significant trends of increase or decrease across inflorescences. Moreover, pollen grain number appeared to follow a Brownian Motion model of evolution. Taken together, these data suggest that pollen grain number is not under strong selection.

Ovule numbers strongly differed between species with rewarding and deceptive flowers. Deceptive flowers contain more ovules than rewarding flowers (Sonkoly *et al.*, 2016; this study), which is possibly an adaptation that enables deceptive

Table 1. *Mean pollen and ovule numbers, pollen-to-ovule ratios and variances thereof in the eight species studied and a comparison with previously published values. Mean low., mean number of ovules on bottom flowers of inflorescences; SE, standard error;* N, *sample number; Var, variance. From lit., values from published literature.*

Species	Pollen grain number				Ovule number					Pollen: Ovule ratio				Deceptive (D)/ Rewarding (R)
	Mean	SE	*N*	From lit.	Mean	SE	Mean low.	*N*	From lit.	Mean	SE	Var	From lit.	
Anacamptis morio	104817	3207	6	–	7347	952	9827	9	>4000[b], 4770 ± 1856[c] 5052[d], 4978 ± 521[m]	18	2.9	49	13[a]	D[k]
Anacamptis pyramidalis	74013	2407	8	–	3435	232	4350	11	1935[b], 3036[d] 2262 ± 205[m]	24	1.7	22	–	D[h]
Dactylorhiza fuchsii	51917	4075	6	–	2659	327	3413	8	6200[f], 3294 ± 774[b] 5205 ± 914[m]	25	5.0	152	21[a]	R[j]
Dactylorhiza incarnata	79113	2761	8	194748[g]	6715	846	9030	11	7270[d,e] 7756[g] 7076 ± 881[m]	13	1.7	23	12.6 (25.2)[g]	D[k]
Dactyorhiza majalis	72050	2422	10	–	4528	455	5447	12	9639 ± 421[m]	19	2.2	46	–	D[l]
Dactylorhiza viridis	35588	2823	8	–	1413	134	1772	12	1339 ± 693[b] 1453 ± 136[m]	29	4.3	147	–	R[j]
Orchis militaris	176417	26062	6	–	12616	1296	14183	7	10948 ± 3274[m]	15	2.2	30	–	D[k]
Platanthera bifolia	215978	25687	6	217396 g	3779	514	4930	6	3666[d,e] 4004[g] 6146 ± 325[m]	59	5.4	175	27.1 (54.3)[g]	R[k]

[a] Neiland and Wilcock (1995); [b] Salisbury (1942)*; [c] Jersáková and Kindlmann (1998)*; [d] Nazarov (1995)*; [e] Nazarov (1998)*; [f] Darwin (1862)*; [g] Nazarov and Gerlach (1997); [h] Daumann (1941); [i] Claessens and Kleynen (2011)*; [j] Dafni and Woodell (1986) – reward as sugary stigmatic exudate; [k] Inda *et al.* (2012) and references therein; [l] Hansen and Olesen (1999); [m] Sonkoly *et al.* (2016)*. * Indicates that ovules were counted as seeds in these studies.

inflorescences to have the same seed set as rewarding inflorescences, despite lower fertilization rates (Sonkoly *et al.*, 2016). Ovule numbers did not show any phylogenetic signal, possibly due to high homoplasy in this character state, i.e. rapid evolution in adaptation to different reproductive ecologies. In both rewarding and deceptive species, ovule numbers decreased from the bottom to the top of the inflorescences.

Due to the lack of differences in pollen grain numbers and strong differences in ovule numbers across pollination strategy and positions in inflorescence, differences in P:O were driven by ovule numbers. Increases in P:O from bottom to top of inflorescences have been observed in orchids (Salisbury, 1942; Nazarov and Gerlach, 1997; Kopylov-Gus'kov Yu *et al.*, 2006), and other taxa (see e.g. Thomson, 1989). Significant differences in variance of P:O between deceptive and rewarding flowers and the well-supported strong phylogenetic correlation of these two characters (P:O variance and pollination strategy) highlight the differences in constraints acting on the reproductive investment in deceptive versus rewarding species. Given that deceptive flowers contain significantly more ovules than rewarding flowers (Sonkoly *et al.*, 2016; this study), and given that usually only the lower flowers on the inflorescences of deceptive flowers are fertilized (Nilsson, 1980; Vogel, 1993; Jersáková and Kindlmann, 1998), it seems likely that deceptive inflorescences are under a strong constraint to stringently decrease ovule numbers from bottom to top of the inflorescence in order to efficiently allocate resources. In rewarding flowers there are much fewer ovules, and fertilization occurs across the whole inflorescence. It thus seems likely that the constraints acting on reproductive allocation in rewarding inflorescences are much weaker, which could explain the much larger variance in P:O found in rewarding inflorescences.

Ultimately, the new tools that we present will allow much broader comparative studies of the diverse groups of angiosperms in which pollination by deceit takes place, and will allow us to better quantify plant reproductive investment.

Supplementary data

Supplementary data are available at *JXB* online.

Data S1. Details of the choice of ANOVA test.

Appendix S1. Loss of contrast of developing seeds in selected European orchid species and comparison with *Arabidopsis thaliana*.

Table S1. Details of the species collected, locality, collection date, breeding strategy, pollinators, and permits.

Table S2. Computed tomography scanning parameters.

Table S3. Counts of pollen grains, massulae, and ovules.

Table S4. Phylogenetic signal estimates of the maximum likelihood values of Pagel's λ for continuous traits and the symmetric model for a discrete trait.

Table S5. Phylogenetic generalized least-squares analysis for four models with coefficients for predictors.

Fig. S1. Lack of homogeneity in ovule distribution.

Movie S1. 3D models of subset data from high-resolution scans of a pollinium for each step of image processing, from raw reconstructed data to machine-countable objects.

Acknowledgements

The authors would like to thank Manuel Pimentel and Luis Ángel for sharing their phylogenetic tree file. We would also like to thank Manfred Fischer, whose encyclopedic knowledge of the Austrian flora made this project possible, and Luise Schratt-Ehrendorfer and Harald Niklfeld for their help in planning and carrying out the field work.

References

Ackerman JD. 1986. Mechanisms and evolution of food-deceptive pollination systems in orchids. Lindleyana **1,** 108–113.

Anderson MJ. 2001. A new method for non-parametric multivariate analysis of variance. Austral Ecology **26,** 32–46.

Aronne G, Cavuoto D, Eduardo P. 2001. Classification and counting of fluorescent pollen using an image analysis system. Biotechnic & Histochemistry **76,** 35–40.

Bechar A, Gan-Mor S, Vaknin Y, Shmulevich I, Ronen B, Eisikowitch D. 1997. An image-analysis technique for accurate counting of pollen on stigmas. New Phytologist **137,** 639–643.

Bellaire A, Ischebeck T, Staedler Y, Weinhaeuser I, Mair A, Parameswaran S, Ito T, Schönenberger J, Weckwerth W. 2014. Metabolism and development – integration of micro computed tomography data and metabolite profiling reveals metabolic reprogramming from floral initiation to silique development. New Phytologist **202,** 322–335.

Bolte S, Cordelières FP. 2006. A guided tour into subcellular colocalization analysis in light microscopy. Journal of Microscopy **224,** 213–232.

Burgeff H. 1936. Samenkeimung der Orchideen und Entwicklung ihrer keimpflanzen: mit einem anhang uber praktische orchideenanzucht. Jena: Gustav Fischer.

Candell S. 2009. CT scaling instructions. Carl Zeiss X-Ray Microscopy, Inc.

Charnov EL. 1979. Simultaneous hermaphroditism and sexual selection. Proceedings of the National Academy of Sciences, USA **76,** 2480–2484.

Claessens J, Kleynen J. 2011. The flower of the European orchid. Form and function. Published by the authors. http://www.europeanorchids.com/index.php/en/

Costa CM, Yang S. 2009. Counting pollen grains using readily available, free image processing and analysis software. Annals of Botany **104,** 1005–1010.

Dafni A, Woodell S. 1986. Stigmatic exudate and the pollination of *Dactylorhiza fuchsii* (Druce) Soo. Flora **178,** 343–350.

Darwin CR. 1862. On the various contrivances by which British and foreign orchids are fertilised by insects, and on the good effects of intercrossing. London: John Murray.

Daumann E. 1941. Die anbohrbaren Gewebe und rudimentaren Nektarien in der Blutenregion. Beihefte zum Botanischen Zentralblatt **61A,** 12–82.

DuBois J. 2000. Seed or particle-counting device. Google Patents. http://www.google.com.pg/patents/US6078635

Garamszegi LZ, **ed.** 2014. Modern phylogenetic comparative methods and their application in evolutionary biology. Concepts and Practice. London: Springer.

Hansen I, Olesen JM. 1999. Comparison of reproductive success in two orchids: the nectarless *Dactylorhiza majalis s.s.* and the nectar-producing *Gymnadenia conopsea s.l.* Nordic Journal of Botany **19,** 665–671.

Harder LD, Johnson SD. 2008. Function and evolution of aggregated pollen in angiosperms. International Journal of Plant Sciences **169,** 59–78.

Harmon LJ, Weir JT, Brock CD, Glor RE, Challenger W. 2008. GEIGER: investigating evolutionary radiations. Bioinformatics **24,** 129–131.

Hayat M. 2000. Principles and techniques of electron microscopy. Cambridge: Cambridge University Press.

Hedrén M, Fay MF, Chase MW. 2001. Amplified fragment length polymorphisms (AFLP) reveal details of polyploid evolution in *Dactylorhiza* (Orchidaceae). American Journal of Botany **88,** 1868–1880.

Inda LA, Pimentel M, Chase MW. 2012. Phylogenetics of tribe Orchideae (Orchidaceae: Orchidoideae) based on combined DNA matrices: inferences regarding timing of diversification and evolution of pollination syndromes. Annals of Botany **110,** 71–90.

Jersáková J, Kindlmann P. 1998. Patterns of pollinator-generated fruit set in *Orchis morio* (Orchidaceae). Folia Geobotanica **33,** 377–390.

Jorgensen S. 1967. A method of absolute pollen counting. New Phytologist **66,** 489–493.

Kannely A. 2005. Preparation and quantification of entomophilous pollen using sonication and an area-counting technique. Madroño **52,** 267–269.

Kearns CA, Inouye DW. 1993. Techniques for pollination biologists. Boulder, CO: University Press of Colorado.

Kopylov-Gus'kov Yu O, Vinogradova T, Lyskov D, Volkova P. 2006. Observations on the population of *Epipogium aphyllum* on the Kem-Ludskij archipelago of the White sea. The materials of the White Sea Expedition of Moscow South-West High School 6.

Lloyd DG. 1979. Parental strategies of angiosperms. New Zealand Journal of Botany **17,** 595–606.

Martins EP, Hansen TF. 1997. Phylogenies and the comparative method: a general approach to incorporating phylogenetic information into the analysis of interspecific data. The American Naturalist **149,** 646–667.

Nazarov V. 1989. Small seed and ovule calculation technique with special reference to the Orchidaceae family. Botanicheskki Zhurnal **74,** 1194–1196.

Nazarov V. 1995. Reproductive biology of Crimean orchids, PhD Thesis. St. Petersburg: Komarov Botanical Institute.

Nazarov VV. 1998. Samenproduktivität europäischer Orchideen. I. Methoden zur Bestimmung der Samenzahl. Journal Europaischer Orchideen **30,** 591–602.

Nazarov VV, Gerlach G. 1997. The potential seed productivity of orchid flowers and peculiarities of their pollination systems. Lindleyana **12,** 188–204.

Neiland MRM, Wilcock CC. 1995. Maximization of reproductive success by European Orchidaceae under conditions of infrequent pollination. Protoplasma **187,** 39–48.

Nilsson LA. 1980. The pollination ecology of *Dactylorhiza sambucina* (Orchidaceae). Botaniska Notiser **133,** 367–385.

Oksanen J, Blanchet FG, Kindt R, *et al*. 2013. vegan:. Community Ecology Package, version 2. https://cran.r-project.org/web/packages/vegan/index.html

Okuda S, Tsutsui H, Shiina K, *et al*. 2009. Defensin-like polypeptide LUREs are pollen tube attractants secreted from synergid cells. Nature **458,** 357–361.

Ollion J, Cochennec J, Loll F, Escude C, Boudier T. 2013. TANGO: a generic tool for high-throughput 3D image analysis for studying nuclear organization. Bioinformatics **29,** 1840–1841.

Orme D. 2013. The caper package: comparative analysis of phylogenetics and evolution in R. R package version 5. https://cran.r-project.org/web/packages/caper/vignettes/caper.pdf

Pagel M. 1999. Inferring the historical patterns of biological evolution. Nature **401,** 877–884.

Porsch O. 1909. Neuere Untersuchungen über die Insektenanlockungsmittel der Orchideenblüte. In Mitteilungen des Naturwissenschaftlichen Vereines für Steiermark **45,** 346–370.

Proctor H, Harder L. 1994. Pollen load, capsule weight, and seed production in three orchid species. Canadian Journal of Botany **72,** 249–255.

R Core Team. 2016. R: a language and environment for statistical computing. Vienna, Austria: R Foundation for Statistical Computing. www.r-project.org.

Salisbury EJ. 1942. The reproductive capacity of plants: studies in quantitative biology. London: George Bell & Sons, Ltd.

Schindelin J, Arganda-Carreras I, Frise E, *et al*. 2012. Fiji: an open-source platform for biological-image analysis. Nature Methods **9,** 676–682.

Schneider CA, Rasband WS, Eliceiri KW. 2012. NIH Image to ImageJ: 25 years of image analysis. Nature Methods **9,** 671–675.

Sonkoly J, Vojtkó AE, Tökölyi J, Török P, Sramkó G, Illyés Z, Molnár VA. 2016. Higher seed number compensates for lower fruit set in deceptive orchids. Journal of Ecology **104,** 343–351.

Staedler YM, Masson D, Schönenberger J. 2013. Plant tissues in 3D via X-ray tomography: simple contrasting methods allow high resolution imaging. PLoS ONE **8,** e75295.

Takeuchi H, Higashiyama T. 2016. Tip-localized receptors control pollen tube growth and LURE sensing in Arabidopsis. Nature **531,** 245–248.

Thomson JD. 1989. Deployment of ovules and pollen among flowers within inflorescences. Evolutionary Trends in Plants **3,** 65–68.

Van der Cingel NA. 1995. An atlas of orchid pollination: European orchids. Rotterdam: A. A. Balkema.

Van der Pijl L, Dodson CH. 1966. Orchid flowers: their pollination and evolution. Coral Gables, Florida: Fairchild Tropical Garden and the University of Miami Press.

Vogel S. 1993. Betrug bei Pflanzen: Die Täuschblumen. Mainz, Germany: Abhandlungen der Akademie der Wissenschaften und der Literatur.

Xradia. 2010. MicroXCT-200 and MicroXCT-400 user's guide v. 7.0. Carl Zeiss X-Ray Microscopy, Inc.